'A lot's in a name': Insights from Debates on Thermal and Nonthermal Effects in Plasmonic Catalysis

Joey Offen, Zhijia Geng, Yifan Yu and Jie Liu*

Department of Chemistry, Duke University, Durham, NC 27708, USA.

Abstract

Plasmonic catalysis is uniquely positioned between photo/electrochemistry and thermal chemistry such that multiple factors may compete to dominate the reaction enhancement mechanism. The adoption of norms originating in both photochemistry and thermal chemistry has resulted in the use of language and methods of data analysis, which, in the context of plasmonic catalysis, may be implicitly contradictory. This article tracks several years of research towards understanding thermal and nonthermal effects in plasmonic catalysis and culminates with a discussion on how the choice of language and presentation of data can be tuned to avoid subtle yet significant contradictory implications.

Key Words: Plasmonic Catalysis; Quantum Efficiency; Photothermal Effect; Light Penetration; Heterogeneous Catalysis; Photochemistry; Thermal Gradient

Introduction

Ecological effects of anthropogenic climate change are prompting the adoption of "green" energy sources and accelerating transitions to more energy-efficient processes in many industries. Currently, the chemical industry is a significant contributor to global emissions and faces unique challenges in decarbonizing. Plasmonic catalysis has garnered significant interest in recent years for its efficient use of solar energy to synthesize industrially important chemicals while generating fewer greenhouse gas emissions¹. Through the excitation and decay of the localized surface plasmon resonance (LSPR) of a metal nanoparticle, light is converted into excited electrons and holes, as well as thermal energy, directly at the catalyst surface²⁻⁶. Unique to plasmonic catalysis is that excited carriers can be efficiently generated and transferred at kinetically relevant temperatures, whereas the performance of pure semiconductor photocatalysts generally declines at such elevated temperatures. Further, the directness of this path circumvents intermediate steps present in other solar energy transfer schemes where energy is unavoidably lost. Many articles have been written regarding thermal and nonthermal effects in plasmonic catalysis⁷⁻¹³, and there has been significant debate over the underlying mechanism regarding the relative contribution of the electron transfer pathway compared to the photothermal pathway¹³⁻¹⁶. The nature of the mechanism bears significant implications, since a photoexcited electron transfer mechanism often bears higher or different selectivity compared with thermocatalysis 17-19 and can be used to catalyze reactions that would not occur thermally²⁰ or would require extreme thermal conditions²¹. This article tracks several years of our research into thermal and nonthermal effects in plasmonic catalysis, qualifies metrics and models commonly used and occasionally misused, and presents current conclusions and possible future directions.

The LSPR phenomenon has been studied extensively for decades, first for use in sensing in surface-enhanced Raman spectroscopy (SERS) beginning in the 1970s^{22, 23}, and then finding applications in biomedicine for photothermal therapy and drug delivery ^{24, 25}, but it was not until the late 2000's and early 2010's that research into harnessing the LSPR for catalysis began to garner significant attention^{1, 26-30}, and only in 2021 was the first textbook on the subject, *Plasmonic Catalysis: From Fundamentals to Applications*³¹, published. Yet, research has continued, and this article is in some sense a continuation of

the discussion in Chapter 7, Untangling thermal and nonthermal effects, written by members of our group. The precise role and mechanism of nanoparticles in advanced materials is at times unclear, muddled by a blend of synergistic and/or competitive effects. Additionally, the environment within a photoreactor intermixes quantized phenomena of carrier excitation and charge transfer with bulk kinetic effects more readily understood with classical models. Accurately extrapolating the role of local quantum effects to the larger-scale observed phenomena generally poses a significant challenge. However, in plasmonic catalysis this challenge is greatly compounded by the unique heterogeneity of the reaction environment in a gas-solid photoreactor. Heat is readily transported throughout the catalyst bed, whereas light is not. Thus, the photothermal and nonthermal effects are unevenly distributed, effectively creating separate reaction environments, namely the illuminated surface and the "dark" subsurface⁸. At the illuminated surface, "hot" electrons and holes can be selectively transferred to antibonding orbitals of key reaction intermediates to promote the cleavage of specific bonds¹⁷ or induce desorption by electronic transmission (DIET)^{32, 33} in addition to kinetic photothermal effects or thermal desorption. Past the penetration depth of light, photothermal heating continues to accelerate the reaction. The overall observed enhancement from light illumination has to be studied separately for both environments due to the two different mechanisms, as discussed below.

Discussion

As different catalytic reaction systems respond differently to heat and light, it can be challenging to understand the degree to which phenomena observed in one setting apply to another, as discussed by several groups in their recently publications³⁴⁻³⁶. Research in our group into thermal and nonthermal mechanisms of gas-solid plasmonic catalysis began with the development of a model system possessing both thermal and nonthermal activity, CO₂ hydrogenation to CH₄ on Rh nanoparticles supported on Al₂O₃¹⁷. This was followed by more research into accurately understanding the thermal profile of the reactor through measuring, modeling⁸ and experimental mimicry of photothermal heating barring direct illumination^{37, 38} for a more quantitative separation of thermal and nonthermal effects. The research culminated with the development of a method to quantitatively separate thermal and nonthermal effects largely resilient to deviations in thermocouple accuracy, while also highlighting discrepancies unique to plasmonic catalysis that arise when comparing performance across different reactions and systems. Many studies adopted metrics originating from thermal and photocatalysis, which includes adjusting the rate by the mass of the catalyst and the use of "quantum efficiency (QE)". While these metrics are certainly valuable, the varying and hybrid nature of the enhancements in plasmonic catalysis compared to pure thermal and pure photocatalysis merits more precise language and qualified use. While a semantic discussion may seem trifling to those with experience, precise nomenclature remains an important aspect of scientific communication, especially benefiting newcomers becoming acquainted with the field.

I. Recognition of Nonthermal Effects in a Model System

Research into plasmonic catalysis in our lab began with a publication in 2017 that provided strong evidence for the existence of a nonthermal reaction mechanism occurring on a thermally active catalyst¹⁷. We developed a model system consisting of the reduction of CO₂ over Rh nanoparticles supported on Al₂O₃ to form CH₄ and/or CO. The dramatic difference observed in selectivity between illuminated and unilluminated catalysts gave additional credence to the existence of both mechanisms and made the case that a single catalyst could be dominant in the requisite circumstances. The data in Figure 1 was collected at low conversions to avoid mass transport limitations and in the light-controlled regimen specifically to highlight the presence and role of the nonthermal effect. In addition to a significant enhancement of reaction rate (**Figure 1a**), a dramatic shift in selectivity towards CH₄ was observed (**Figure 1b**).

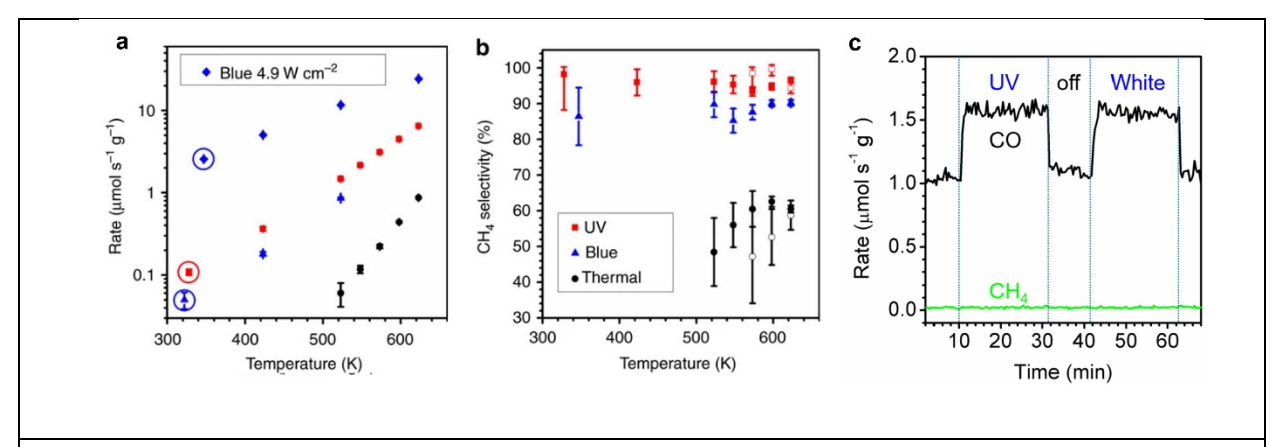


Figure 1. Product selectivity on the Rh and Au photocatalyst. (a) Overall, CH₄ production rates in dark (black circles) and under ultraviolet (UV) (red squares, 3 W cm⁻²) and blue (blue triangles, 2.4 W cm⁻²) LEDs with the same photon flux, and with twice the blue photon flux (blue diamonds, 4.9 W cm⁻²). UV light is more efficient at enhancing the reaction rates than blue light with the same photon flux. Circled points show the unheated steady-state temperatures and reaction rates. Error bars represent the s.d. of measurements by the mass spectrometer. (b) Selectivity towards CH₄ of the thermo- (black circles) and photocatalytic reactions under UV (365 nm, red squares) and blue (460 nm, blue triangles) illumination as a function of temperature under H₂-rich (CO₂:H₂=1:5.5, solid symbols) and H₂-deficient (CO₂:H₂=1:3.1, open symbols) conditions. The photoreaction rates are calculated by subtracting the thermocatalytic reaction rates from overall reaction rates at the same temperature. The photoreactions under ultraviolet light show higher selectivity towards CH₄ than under blue light, which are both much higher than that of the thermocatalytic reaction. (c) Photocatalytic CO production on the Au/Al₂O₃ photocatalyst under UV and white light. The CO₂ hydrogenation reaction at 623 K under ultraviolet and white light of the same intensity (1.18 W cm⁻²) exhibited practically the same reaction rates, and CO was the exclusive product on the Au photocatalyst at these conditions. Reproduced with permission from ref. 17. Copyright 2017 Springer Nature.

A marked change in selectivity upon illumination remains a relatively accessible method to detect the presence of a significant nonthermal mechanism on a thermally active catalyst, requiring neither advanced spectroscopy nor custom equipment 17-19, 39. To ensure selectivity data is unbiased, the conversion rate should be held constant since in a steady state flow reactor, product selectivity at constant rate is directly proportional to product yield⁴⁰. This consistency of kinetic conditions is of particular importance in series reactions where intermediates must be held constant as well³⁹. Therefore, conversion rates were kept below 5% to minimize discrepancies which arise from inconsistent kinetic conditions and to avoid mass-transport limitations¹⁷. While selectivity provides accessible mechanistic insights, it is not a guaranteed path to a complete understanding on its own and can be situationally limited. For example, for CO₂ reduction over Au/Al₂O₃ the reaction produces only CO (Figure 1c), so monitoring selectivity provides no mechanistic clues. For such a reaction with no change in selectivity, a change in apparent activation energy can be evidence for nonthermal effects occurring for the plasmonic Au catalysts. It should be noted that obtaining an accurate activation energy is heavily reliant upon the quality of the thermal data whether collected by thermocouple or optically and is therefore especially vulnerable to errors originating in thermocouple quality, position, and preparation. It can also be complicated by the interaction between the thermocouple and external heating method as well as errors associated with the imperfect application of optical thermometry. At the time of the publication of the article¹⁷, the realization of the differences between the surface layer and the underlayer of the catalyst was not commonly considered, causing interpretation inaccuracy in the original publication. Nonetheless, by measuring the

reaction rates at different temperatures for both illuminated and unilluminated catalysts, apparent activation energy was calculated using an Arrhenius equation. The obtained activation energy was lower for the illuminated catalysts compared to the dark thermal conditions for both Rh (Figure 2 a & b) and Au (Figure 2 c & d), providing additional evidence for the existence of a change in mechanism to one with a reduced energy barrier. The reduction in activation energy for CO production on Au/Al₂O₃ suggests the presence of a nonthermal mechanism even though the selectivity remains entirely towards CO. However, due to potential shortcomings of thermocouple measurements, relying only on activation energies is not necessarily conclusive. Subsequent study from our group focused on obtaining a more accurate understanding of the reactions thermal profile. Even with accurate thermal data, a change in activation energy calculated from Arrhenius plots is not definitive proof of nonthermal mechanism because activation energy itself may change as a function of temperature⁴¹. Therefore, it is conceivable that some change in activation energy could be the result of photothermal heating not properly accounted for in the thermal assessment. More recently, methods of differentiating between different nonthermal effects, including the transfer of carriers generated by intraband transitions, interband transitions, and enhanced electric field effects, have been developed by the Baldi group⁹.

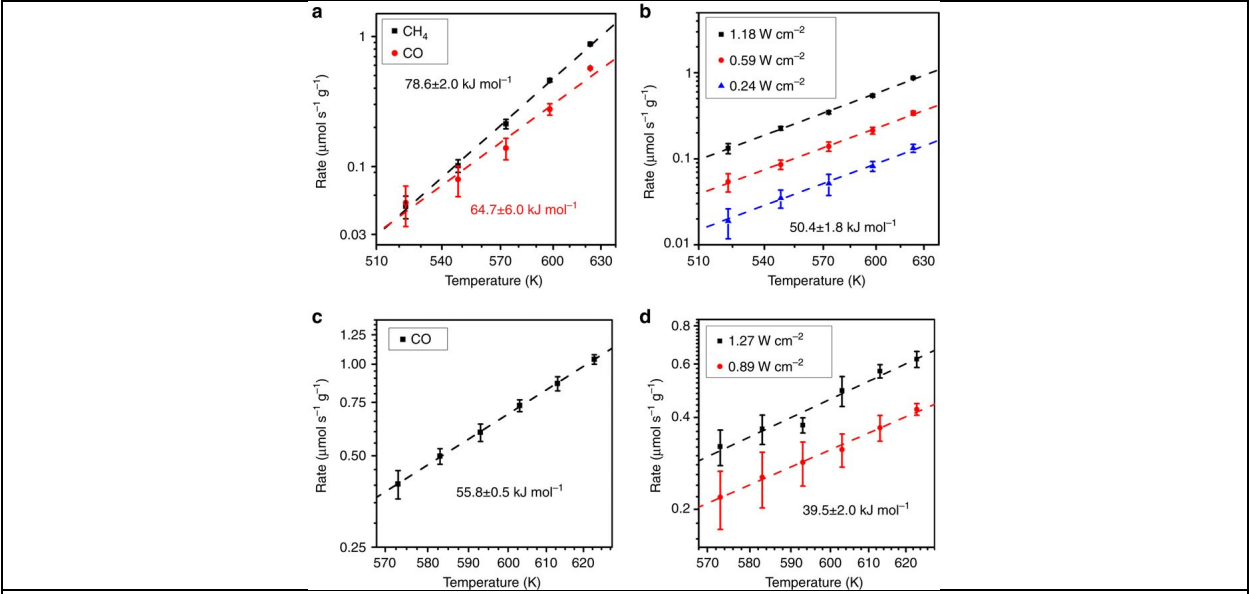


Figure 2. Apparent activation energies on the Rh and Au photocatalysts. (a) Thermocatalytic reaction rates of CH₄ (black squares) and CO (red circles) production on Rh/Al₂O₃ as a function of temperature. The apparent activation energies are obtained by fitting the results with an Arrhenius equation. (b) Photoreaction rates for CH₄ production on Rh/Al₂O₃ under 1.18 (black squares), 0.59 (red circles) and 0.24 W cm⁻² (blue triangles) UV illumination as a function of temperature. The photocatalytic reactions show the same apparent activation energy, which is lower than that of thermocatalytic reaction. (c) Thermocatalytic reaction rates of CO production on Au/Al₂O₃ as a function of temperature. (d) Photoreaction rates of CO production on Au/Al₂O₃ under 1.27 (black squares) and 0.89 W cm⁻² (red circles) white light as a function of temperature. Reduced apparent activation energies of photoreactions are observed on both Rh and Au photocatalysts, but with different selectivity. Error bars represent the s.d. of measurements by the mass spectrometer. Reproduced with permission from ref. 17. Copyright 2017 Springer Nature.

Rounding out this study were DFT calculations (**Figure 3**) to explain the increased selectivity of the nonthermal mechanism of the Rh catalyst towards methane. Computations of the local density of

states (LDOS) of key reaction intermediates on the Rh face revealed the susceptibility of adsorbed CHO, whose dissociation is the rate-limiting step in CH₄ formation⁴², to receiving hot electrons from the Rh catalyst. Computational analysis revealed that the adsorbed CHO intermediate had an increased density of states for the C–O π^* antibonding orbital, with energy ~2eV above the fermi level. As plasmon decay theoretically can create excited carriers with energy up to total photon quantum³¹, ~2eV is well within the range of energies available to an electron photoexcited by the decay of a plasmon generated by an UV or blue source. Also revealed by the DFT calculations was the comparatively weak and broad nature of the CO–Rh antibonding orbital intermediate. Desorption of CO from Rh is the rate-limiting step in the formation of CO⁴², and the computed dearth of states available to receive electrons excited by the LSPR explains why CO production is not similarly enhanced. The weak and broad nature of the CO–Rh orbital does not provide energy states positioned to accept plasmonically generated hot electrons from blue or UV light.

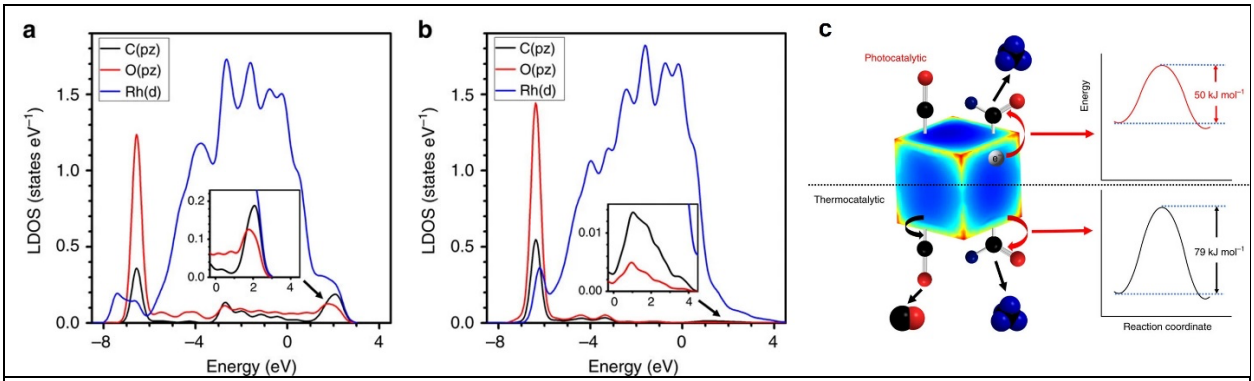


Figure 3. DFT calculations of CHO and CO intermediates on the Rh(100) surface. (a) LDOS for adsorbed CHO on $C(p_z)$, $O(p_z)$, and Rh(d) orbitals. The Rh(100) surface is perpendicular to the x direction, and the C–O bond is along the y direction. Major bands are identified as: (1) C–O π bonding band (-6.5 eV) with $C(p_z)$ (black) and $O(p_z)$ (red) interactions; (2) C–O π^* anti-bonding band (1-3 eV, mode around 2 eV) with $C(p_z)$ and $O(p_z)$ interactions. (b) LDOS for adsorbed CO on $C(p_x)$, $O(p_x)$, and Rh(d) orbitals. The Rh(100) surface is perpendicular to the x direction, and the C–O bond is along the x direction. Major bands are identified as: (1) C–O σ bonding band (-6.3 eV) with $C(p_x)$ (black) and $O(p_x)$ (red) interactions; (2) Very weak Rh–C anti-bonding band (0–3 eV, mode around 1 eV) with $C(p_x)$ and Rh(d) (blue) interactions. All energies are referenced to the Fermi level. The insets are magnified plots of the anti-bonding regions. (c) The thermocatalytic reaction activates both CO–Rh bonds and CH–O bonds to produce CO and CH₄, respectively. Hot electrons generated in the photocatalytic reaction selectively activate the C–O bonds of the CHO intermediate and reduce the apparent activation energy to enhance the CH₄ production rate. The black, red, and blue spheres are carbon, oxygen, and hydrogen atoms, respectively. The red corners of the cube show the intense electric field from the excitation of LSPRs⁴³. Reproduced with permission from ref. 17. Copyright 2017 Springer Nature.

Thus, the nonthermal mechanism was confirmed theoretically and experimentally to dramatically enhance only the CH₄ pathway (**Figure 3c**), effectively shifting the selectivity almost entirely to methane. This study¹⁷ showcased the transformative impact of nonthermal effects on reaction rate and selectivity while maintaining the existence of the thermal mechanism, qualitatively confirming the existence of both and showing that the hot-electron mechanism can dominate at high light intensity. However, in retrospect, the temperature measurements in this study relied on a single thermocouple far from the catalyst surface, potentially jeopardizing the absolute accuracy of analyses heavily reliant on accurate thermal data such as activation energy. While the selectivity analysis of the nonthermal reaction is less sensitive to thermocouple effectiveness and the resulting precision of temperature data, accurate knowledge of the surface temperature remains vital for quantitative metrics sensitive to variable thermal conditions, such as

Arrhenius analysis to obtain activation energies, and "QE" measurements, which may be subject to or even misappropriate thermal effects. Spatially precise thermal data is especially desirable for reactions that did not provide pronounced and sharp changes in selectivity or other such mechanistic clues comparatively more resistant to local temperature variations.

II. Accurate Characterization and Modeling of the Thermal Environment

To obtain a more complete understanding of the catalyst temperature in our subsequent studies, two additional thermocouples, T_1 and T_2 , were embedded into the catalyst bed, with T_1 located just beneath the surface and T_2 at the bottom of the bed (**Figure 4a**)⁸. The singular thermocouple used for previous experiments T_c remained in its original position between the reaction chamber and the external heating element. As UV LED illumination approached 3 W/cm², the new thermocouples revealed a temperature gradient over 100 °C between the surface and the bottom of the catalyst bed (T_1 and T_2) (**Figure 4b**) for a given a chamber temperature (T_c). This pronounced gradient occurred in a catalyst bed merely 3mm thick. To accurately characterize thermal reactivity in the nonuniform thermal environment and allow for facile separation and comparison of thermal and nonthermal effects among varying thermal and optical conditions, a signal descriptor "equivalent temperature," T_c , was developed to create a uniform descriptor using a simplified one-dimensional thermal profile bundling together thermal effects from the multitude of sources present in the reaction environment⁸:

$$e^{-E_a/kT_e} = \frac{1}{T_2 - T_1} \int_{T_1}^{T_2} e^{-E_a/kT} dT$$
 (1)

The recursive format allows for the iterative calculation of apparent activation energy (E_a) to the point of convergence from an initial E_a estimate, calculated using $T = T_1$. A subsequent activation energy corresponding to the respective thermal and nonthermal regions can be calculated using the dark reaction rate and T_1 and T_2 values plugging in the initial E_a , with the appropriate T_1 and T_2 data to obtain T_e . T_e can then be used with T_1 and T_2 and the most recent E_a to compute a new E_a , and so on until E_a converges producing an accurate activation energy for the thermal reaction occurring throughout the depth of the catalyst bed as function of surface and base temperature. This dark E_a paired with the illuminated T_1 and T_2 , can then be used to calculate T_e under illumination implicitly accounting for the thermal contributions under illumination including photothermal heating and heat released by the exothermic reaction. Once the thermal contribution is isolated it can be subtracted from the total illuminated rate to obtain the nonthermal rate. Thus, the separation of thermal and nonthermal effects was improved by accounting for surface photothermal heating and heat released from the exothermic reaction.

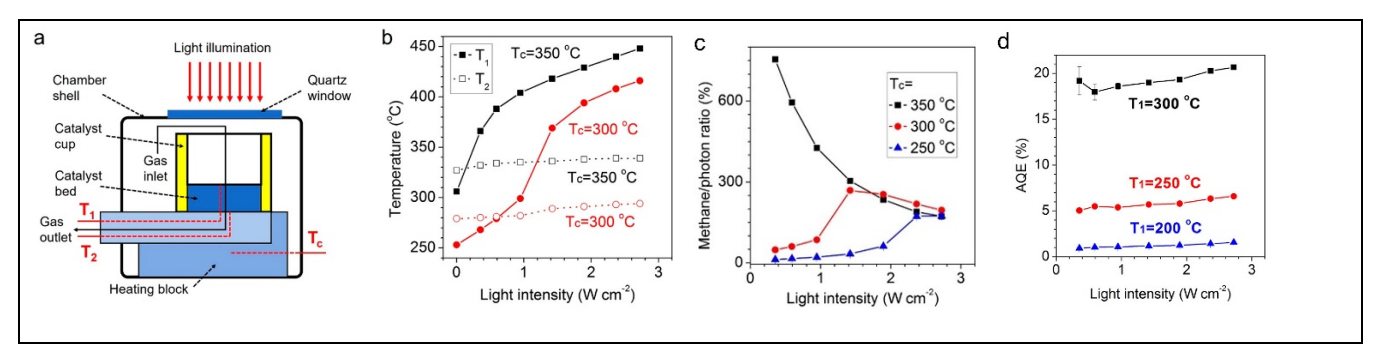


Figure 4. Improvements to thermal characterization and effect on photo efficiency data. (a) Schematic representation of the modified reaction chamber for in situ measurements of top- (T_1) and bottom- (T_2) surface temperatures of the catalyst bed. Chamber temperature (T_c) is measured by a thermocouple underneath the catalyst cup inside the heating block. (b) Measured T_1 (solid symbols) and T_2 (open symbols) at $T_c = 350$ °C (black squares) and 300 °C (red circles) as a function of I_{UV} (c) CH₄/photon ratios at the same T_c temperatures as a function of I_{UV} . The CH₄/photon ratio is calculated as the difference between CH₄ production rate under light and in the dark at the same T_c , divided by photon flux. The reactions are carried out with a ~3 mm thick Rh-s/TiO₂ catalyst and 50 sccm CO₂, 150 sccm H₂, and 50 sccm Ar. Error bars are smaller than symbols and represent the standard deviation of measurements by the mass spectrometer. (d) AQE for $T_1 = 300$ °C (black squares), 250 °C (red circles), and 200 °C (blue triangles) as a function of I_{UV} Error bars represent the standard deviation of measurements by the mass spectrometer. Reproduced with permission from ref. 8 Copyright 2018 American Chemical Society.

Careful parsing of thermal and nonthermal effects provided insight into a weakness of the commonly used metric of "QE," where the nonthermal rare (or, in cases where the two have not been separated, the total rate) is divided by the photon flux. While this straightforward index provides useful information on photoefficiency, it can be a misnomer attributing classical thermal effects to quantum carrier excitation and transfer mechanisms. An unsubtle example of this issue can be seen in Figure 4c, where the QE reached an unreasonable 800%. Despite being generally known as QE, it has been labeled in Figure 4c as CH₄/photon to avoid misattributing the mechanism. This extreme case highlights the issues of QE measurements and invokes a semantic argument. In the case of photovoltaics, where the metric originated, the energy of a photon is singularly transferred to an electron, resulting in an interband excitation, followed by thermal relaxation to the bottom of the conduction band and subsequent transfer to a neighboring material. Here, an increase in the temperature is detrimental, indicated by the negative temperature coefficient of PV devices, due to increases in decay rates depleting the population of excited carriers prior to transfer⁴⁴. Given the research efforts towards efficient cooling of PV to maintain optimal performance⁴⁵, there is no risk of mischaracterizing thermal effects as quantum phenomena, as the negative impact far outweighs any benefit. However, in plasmonic catalysis, where the mechanism of carrier excitation and transfer continues to perform well under commonly studied conditions and thermal kinetic effects may still enhance an excited electron transfer mechanism, labeling the metric "quantum" may unnecessarily misappropriate thermal effects. Thus, while unproblematic in its native context, QE could be rephrased to more inclusive language for use as the standard photoefficiency index in plasmonic catalysis.

III. A More Resilient Method and the Implications of Nomenclature

While the scenario in **Figure 4c** is especially egregious, there may be other scenarios where the misappropriation is less readily apparent. Given the increased scrutiny that has recently been placed on the thermal and nonthermal debate, such occurrences may be decreasing in frequency but could still plausibly go unnoticed. Indeed, as is evident in **Figure 4d**, even though the percent efficiency has been made more reasonable, it still depends heavily upon temperature and therefore may potentially contain

some thermal effects, albeit less than that in **Figure 4c**. To avoid potential misappropriation, we previously argued for the qualification of the nomenclature renaming "QE" to "apparent quantum efficiency (AQE)". However, the possibility remains that, even in AQE, thermal effects are present; therefore, there is reason to go further by introducing a new index: "overall light effectiveness" (OLE)⁴⁶, as defined by:

OLE
$$(\mu \text{mol} \cdot \text{s}^{-1}/\text{W} \cdot \text{cm}^{-2}) = \frac{\text{Total production rate enhanced by light } (\mu \text{mol} \cdot \text{s}^{-1})}{\text{Light intensity } (\text{W} \cdot \text{cm}^{-2})}$$
 (2)

Omitting the word "quantum" circumvents the possibility of mischaracterizing classical thermal effects with quantum mechanical electron excitation and transfer while still conveying important information about the efficiency of the utilization of the light's energy. OLE's inclusive nature makes it more accurate and appropriate for most if not all plasmonically catalyzed reactions. Additionally, by not normalizing the index by the mass of catalyst, OLE can account for both photothermal and nonthermal effects which have different dependence on the catalyst mass. Catalyst mass is one of several major factors that distinctly and interdependently impact photoefficiency in plasmonic catalysis, and changing the mass of the catalyst adjusts the balance between nonthermal effects that are exclusively on the surface and thermal effects present thought the entire bulk⁴⁶. It was found that plotting OLE as a function of a single major variable in a variety of conditions (Figure 5), including for varying masses (Figure 5a), made each individual effect more apparent and facilitated combined optimization of all tunable variables compared to using the rate alone or the rate adjusted-per-mass catalyst, which can mask useful information about the relative significance of thermal and nonthermal effects⁴⁶. Thus, adjusting by catalyst mass can be counterproductive, as it implies uniformity across the entire mass, and in plasmonic catalysis, uniformity of reaction conditions is rare due to the difference in penetration depth between light and heat. As a result, even when using only a few milligrams of catalyst, there may still exist two extremely different environments: the illuminated surface, where both thermal and nonthermal effects contribute, and the dark region beneath, where only thermal effects penetrate.

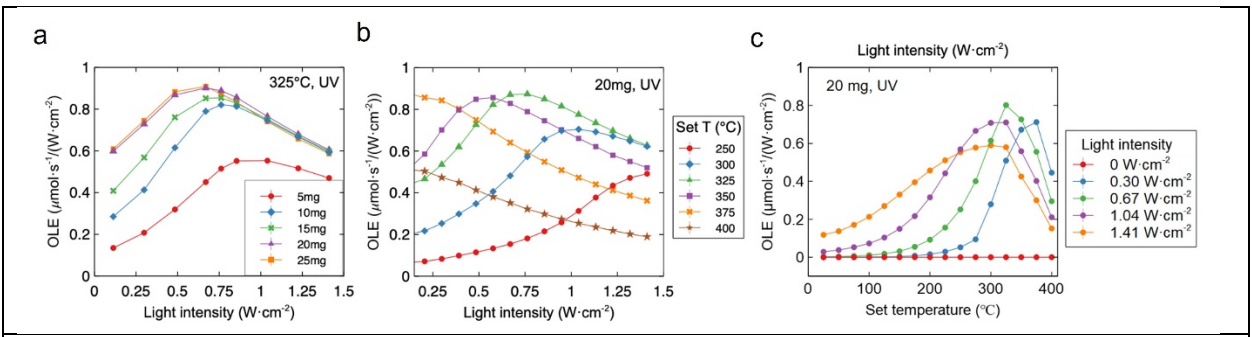


Figure 5. OLE as function of set temperature, intensity, and mass. (a) OLE with varying amount of catalysts: (b) at different set temperatures, and (c) as a function of set temperatures with 20mg catalyst under different light intensities of UV light. Reproduced with permission from ref. 46. Copyright 2023 Springer Nature.

This dynamic can be exploited to distinguish thermal and nonthermal effects in a manner especially resilient to errors associated with measuring catalyst temperature profile in high spatial resolution⁴⁶. Simply by varying the mass of the catalyst, the thermal and nonthermal effects can be separated. The mass dependence test operates on the principle that, due to the shallow penetration depth of light into the powdered catalyst, the nonthermal effects are limited to the illuminated surface layer (**Figure 6a**)⁴⁶. However, thermal effects are present on both the surface and throughout the entire bulk of

the catalyst, as heat is readily distributed between adjacent particles in good contact. By replacing increasing fractions of the catalyst with inert material while maintaining a layer of pure catalyst on top, the total rate is diminished, whereas the nonthermal rate remains unchanged (**Figure 6b**). Thus, the entire rate decrease can be attributed to the thermal effects of light holding the nonthermal effect constant. After performing this exercise to the limit of human precision, in this case a surface layer of 2.5 mg of pure catalyst, the trend can be mathematically extrapolated to zero thickness, i.e., the *y* intercept on plot of rate vs. mass of pure catalyst (**Figure 6c**) to obtain the nonthermal rate which can then be subtracted from the total rate to give the thermal rate⁴⁶. Similarly, the independence of AQE from catalyst mass indicated that it encompassed activity only on the catalyst surface and therefore was a suitable measure for nonthermal activity (**Figure 6d**). While nonthermal effects certainly dominate the surface in this case, thermal effects should not be entirely excluded and are considered to be present in the surface in the mass-dependent analysis⁴⁶.

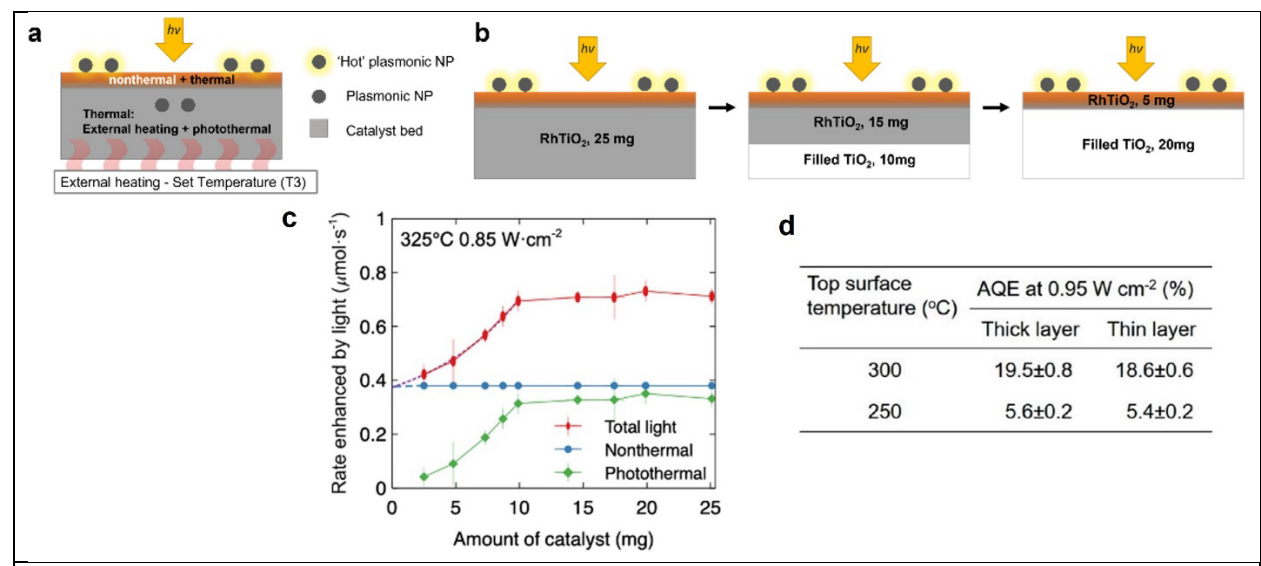


Figure 6. Mass dependence tests. (a) Schematic diagram of catalyst bed under direct light illumination. (b) Schematic illustration of mass-dependence test. (c) The calculated light-enhanced rate, nonthermal rate, and photothermal rate under 325 °C, 0.85 W·cm² extracted by varying the amount of catalyst to change only the thermal rate while the nonthermal rate remains constant. (d) AQE from a ~3 mm and a ~1 mm thick Rh-s/TiO₂ catalyst for $T_1 = 300$ and 250 °C for $I_{UV} = 0.95$ W cm⁻². Varying the mass does not change AQE beyond the experimental error, indicating that it captures only surface effects. (a), (b), & (c) Reproduced with permission from ref. 46. Copyright 2023 Springer Nature. (d) Reproduced with permission from ref. 8. Copyright 2018 American Chemical Society.

Perhaps a holdover from the field of thermocatalysis, adjusting performance metrics by mass in plasmonic catalysis may result in useful information being overlooked, without necessarily facilitating accurate comparisons between different experiments. In its native context of thermal catalysis, adjusting by mass makes obvious sense, since in the proper kinetic conditions the entirety of the catalyst operates in essentially the same environment. And from an economics point of view, it makes sense to adjust for cost. However, if one is to adjust for amount of catalyst used, for a predominately nonthermal reaction it may make more sense to adjust for illuminated surface area, akin to the common practice in electrochemistry, where catalytic performance is generally adjusted by electrode area, or study of photovoltaics, where performance is adjusted per illuminated area by using a set of standardized conditions (STC)⁴⁷. By normalizing nonthermal performance only by illuminating power and area, OLE accounts for the extreme heterogeneity of the plasmonic catalytic environment. Additionally, by focusing solely on energy input and not adjusting for the energy difference between photons of different wavelengths, OLE lends itself

well to maximizing combined thermal and nonthermal performance across both white light and monochromatic illumination, a benefit for solar applications.

Figure 7a shows the nonthermal effect as a function of light intensity, with T_c set to 325 °C for 20 mg of catalyst. These conditions were chosen as, across the different conditions measured in Figure 5, OLE peaked between 300 and 400 °C for all measured intensities (Figure 5c)⁴⁶. The nonlinear trend for the nonthermal rate with respect to light intensity (Figure 7a) beckons a discussion, as hot-carrier generation has been theorized to vary linearly as a function of light intensity in spherical plasmonic nanoparticles³. Yet, a nonlinear relationship between intensity and nonthermal rates has been observed even after the exclusion of significant thermal effects^{7,48}. Several theories have been developed suggesting that, even if hot-carrier generation has a linear relationship with light intensity, other factors involved in carrier transfer from catalyst to adsorbate could be exponentially associated with light intensity. The original hypothesis by Christopher and Linic was that reaction rate could have a nonlinear relationship to light intensity if product desorption was induced by multiple electron transfers²⁷. The role of "hot" electrons in the mechanism was to form a transient negative ion (TNI) with adsorbed product inducing its desorption via desorption by electron transfer (DIET)²⁷. At low light intensities, this rate has a linear function of illumination intensity. However, at higher intensities, the relationship became exponential²⁷. The transition from a linear to a superlinear regimen occurred when the intensity was high enough that the frequency of excited electron scattering events significantly exceeded the inverse of the TNI lifetime²⁷. The probability of two electrons scattering into the metal adsorbate orbitals would then be a function of the probability of both events occurring and therefore be nonlinear²⁷. It was noted that, due to the short TNI lifetime, a singular nanoparticle might struggle to supply enough energetic electrons for such frequent scattering²⁷. However, a nanoparticle cluster has a significantly larger absorption cross section and a significantly enhanced local electric field. The enhanced absorption cross section could supply more photons, and the enhanced local electric field could enhance TNI formation and charge transfer efficiency, allowing a cluster of nanoparticles to achieve the requisite scattering rates even though a single particle could not²⁷. However, this mechanism relies upon particle clustering, and another study found that catalysts with commonly used low mass loadings (<5%) have too low a particle density to support a significant degree of cluster formation⁴⁹. Research supporting multielectron transfer mechanisms through the use of rapid multihole scavengers⁵⁰ provided more evidence for a multicarrier transfer mechanism, and multitransfer mechanisms remain a popular explanation for the frequently observed superlinear relationship^{50, 51}. Alternatively, single-electron transfer mechanisms could still play a role in superlinear response by linearly affecting the concentration of a higher-order absorbate. Plasmonic nonthermal desorption has been shown to significantly affect reaction selectivity⁴⁸ and rate^{21, 48}. If an intermediate, such as adsorbed hydrogen, has a sufficiently negative reaction order for the subsequent step rate-determining step⁸, accelerating its desorption may contribute to a superlinear nonthermal rate dependance on intensity.

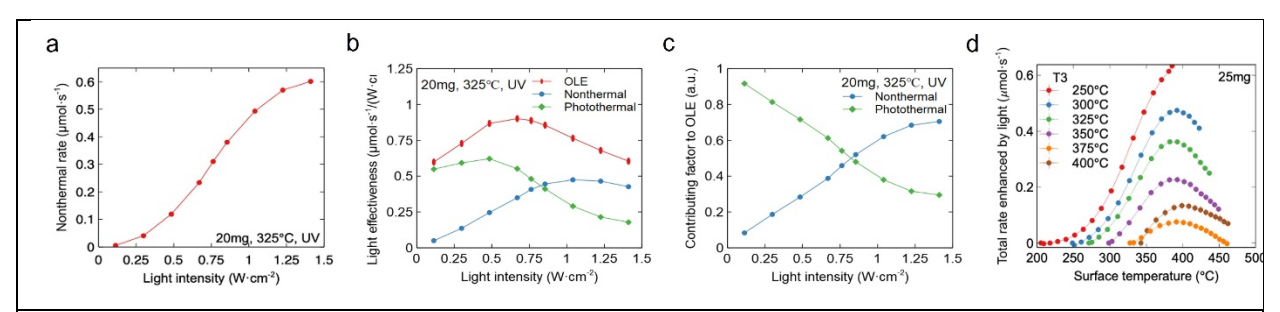


Figure 7. Contributions from nonthermal and photothermal effects to the OLE. (a) The relationship between different light effectiveness, including overall, nonthermal, and photothermal ones and light intensity, and (b) the contributing factors from nonthermal and photothermal effects to the OLE with 20-mg catalyst at 325°C under UV light. Nonthermal and photothermal contributions were obtained through the mass-dependence method depicted in Figure 6. (c) The extracted nonthermal rate as a function of light intensity with 20-mg catalyst at 325°C under UV light. (d) The relationship between measured surface temperature and total rate enhanced by light. Reproduced with permission from ref. 46. Copyright 2023 Springer Nature.

Despite the interest, excitement, and evidence surrounding nonthermal explanations, there also remains evidence that the role of classical thermal effects may at times be overlooked⁵². Our results from parsing OLE into its photothermal and nonthermal components (Figure 7b) and comparing their relative contributions (Figure 7c) suggest that thermal effects may be the source of the superlinear trend in this catalytic system 46. In the conditions where the rate increased exponentially i.e., below 0.67 W·cm⁻², photothermal contributions were found to outweigh nonthermal ones. Further, the rate enhancement of light reached its maximum effectiveness at 0.67 W·cm⁻² within the region where the photothermal contribution to OLE remained the majority factor. Once photothermal and nonthermal contributions to light efficiency were approximately equal, the nonthermal rate reached an inflection point and began to plateau. By the intensity at which the nonthermal contribution was dominant, the effectiveness of light was declining (Figure 7b). This decline is attributed to the theoretical weakening of the plasmonic effect at the high temperatures existing on the surface at intense illumination and high reactor chamber temperature (Figure 7d). As the reactor temperature increased, the peak OLE shifted to lower intensities (Figure 5b), supporting this conclusion. Thus, the "nonthermal" effects are not "athermal". Even if the reaction is promoted via excited carrier transfer far beyond what would be possible under dark thermal conditions alone, classical photothermal effects can still significantly accelerate or decelerate reaction rates. Therefore, it can be concluded that the synergy between thermal and nonthermal effects should be optimized to achieve maximum performance in plasmonic catalysis and that OLE facilitates the optimization process while circumventing the risk of mislabeling classical thermal effects⁴⁶.

IV. A Case Study on a Purely Photothermal Reaction System

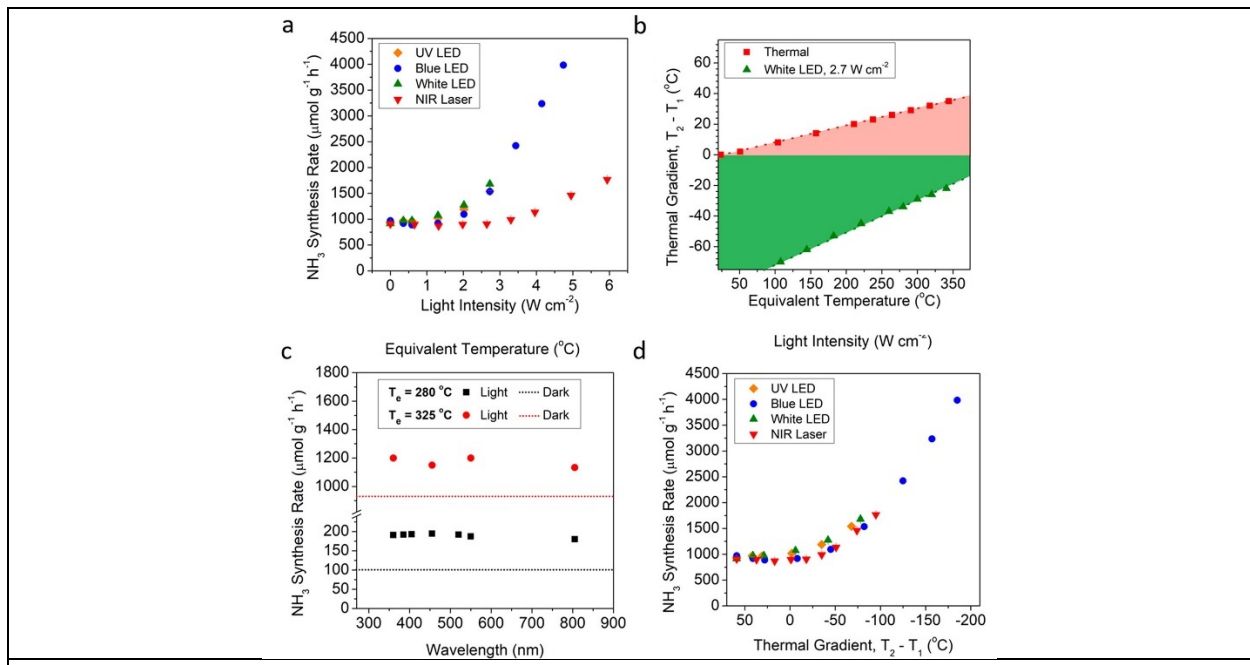


Figure 8. Effect of thermal gradients in plasmonic ammonia synthesis. (a) Measured NH₃ synthesis rates on Ru-Cs/MgO as a function of light intensity for $T_e = 325$ °C using UV (orange diamonds), blue (blue circles), and white (red triangles) LEDs and the NIR laser (green inverted triangles). UV and white LEDs have a maximum intensity of 2.72 and 2.84 W cm⁻², respectively. (b) Measured thermal gradients under dark thermal (red squares) and heated white light illumination (2.7 W cm⁻², green triangles). (c) Measured wavelength-dependent NH₃ synthesis rates ($\nabla T < 0$) with T_e set at 280 °C (black squares) and 325 °C (red circles), compared to dark thermal rates (dotted lines, $\nabla T > 0$). (d) Measured NH₃ synthesis rates as a function of the thermal gradient for $T_e = 325$ °C. Error bars are smaller than symbols and represent the s.d. of measurements by the mass spectrometer. Reproduced with permission from ref. 38. Copyright 2019 American Chemical Society.

Indeed, some plasmonic reactions, which at first appeared to contain nonthermal effects, ended up being entirely photothermally driven such as in the case of NH₃ synthesis on Ru-Cs/MgO³⁸. Plotting the synthesis rate as a function of intensity for a range of different wavelengths showed a stronger enhancement for UV and visible wavelengths compared to IR (**Figure 8a**), which might suggest that once a certain energy threshold was surpassed an electron transfer would occur, as is commonly seen in photocatalysis. With illumination heating the bed surface and the reactor heating element heating from beneath thermal gradients, measured as bottom temperature (T_2) – top temperature (T_1), ranging from –80 °C to +40 °C were observed³⁸. For the given equivalent temperature (T_2) described earlier, turning on the light shifted the gradient approximately 60 °C (**Figure 8b**). However, plotting the data with respect to equivalent temperature, designed to account for non-isothermal conditions, the wavelength dependence disappears C (**Figure 8c**). Rather, instead of there being a hot-electron mechanism, IR wavelengths penetrated deeper into the catalyst bed and therefore created a less pronounced thermal gradient. Plotting the production rate directly as a function of thermal gradient confirmed that once adjusted for the gradient there was no wavelength dependent effect (**Figure 8d**)³⁸.

Accurate thermal data can be a key part of the mechanistic puzzle, as light-induced thermal gradients can significantly affect performance by manipulating the concentrations of reaction intermediates and products to achieve the optimal concentrations given kinetic considerations, effectively shifting the global equilibrium⁵³. While this methodology is most commonly associated with chemical engineering of industrial reactors⁵³. in this case it was found to have pronounced effects on lab-scale experiments of NH₃ synthesis on 20mg of Ru-Cs/MgO catalyst only 3mm deep. As the reaction is reversible, high temperatures accelerate both forward and reverse reactions. In the presence of a temperature gradient, thermophoretic force moves molecules from the higher temperature region to the lower temperature region⁵⁴. By maintaining a colder region immediately behind the hot surface, thermophoretic forces will align with the direction of gas flow, accelerating newly formed NH₃ to the cold regions preserving it from decomposition. Thus, the light-induced gradient shifts the global equilibrium towards the forward reaction.

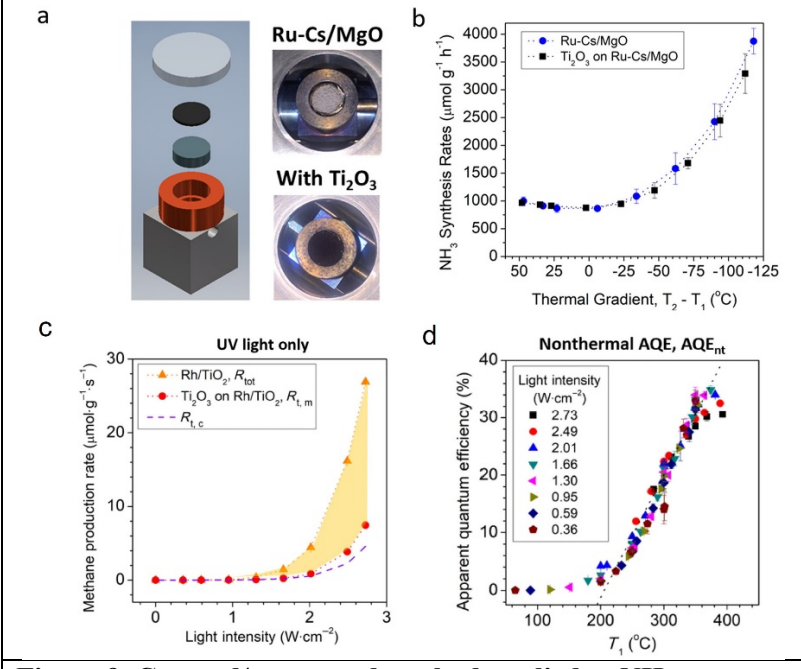


Figure 9. Covered/uncovered method applied to NH₃ synthesis and CO₂ hydrogenation. (a) Schematic for direct and indirect photothermal heating along with photographs of the Ru-Cs/MgO catalyst without and with a top layer of Ti₂O₃. (b) Measured NH₃ synthesis rates as a function of the thermal gradient for $T_e = 325$ °C for direct (blue circles) and indirect (black squares) illumination and photothermal heating of Ru-Cs/MgO by the blue LED. (c) Measured total CH₄ production rate (R_{tot}) for unheated, UV light only (orange triangles) is shown as a function of UV light intensity. Calculated (R_{t,c}) thermal CH₄ production rates are based on corresponding T_e (purple dashes). Measured ($R_{t,m}$) thermal CH₄ production rate from indirectly illuminated Rh/TiO₂ for identical T_1 and T_2 temperatures (red circles). The yellow shaded region represents the nonthermal contribution. (d) Nonthermal AQE of CO₂ hydrogenation as a function of T_1 for varied I_{UV} . (a), (b) & (d) Reproduced with permission from ref. 38. Copyright 2019 American Chemical Society. (c) Reproduced with permission from ref. 37. Copyright 2019 Springer Nature.

To confirm this conclusion, a novel method was employed to emulate the light-induced thermal gradient without direct illumination. A thin layer of Ti_2O_3 , an inert dark black powder, was placed atop the catalyst (**Figure 9a**)³⁸. This powder efficiently absorbed the incident light, converting it to heat across a broad spectrum of wavelengths. When covered by Ti_2O_3 , both the thermal gradients and the performance were the same for the uncovered catalyst (**Figure 9b**), confirming that the rate enhancement was purely a gradient effect. This covered/uncovered method was also effective at parsing thermal from nonthermal effects for a reaction with a significant non-thermal pathway, namely the previously discussed CO_2 hydrogenation on TiO_2 ³⁷. The thermal rate obtained with this method showed reasonable agreement with the calculated thermal rate, and the significant difference between the total rate and thermal rate

confirmed the role of nonthermal mechanism in this catalyst. From this method, a similar conclusion can be drawn that, at high light intensities and low temperatures, nonthermal effects dominate for this catalyst (**Figure 9c**). The calculated AQE was also consistent with the trend observed from OLE using the mass dependence method where at high surface temperatures the photoefficiency declines. Indeed, the relationship between thermal and nonthermal effects explored in this study directly motivated the development of OLE and the mass dependence method.

These observations and analyses encourage a discussion on what the "quantum" in quantum efficiency means in the context of plasmonic catalysis. Does it describe the efficiency of a process that can only be described using quantum mechanics; or is it merely the efficiency per quanta of light? Given its original use to describe an electron-hole excitation and transfer process a purely photothermal mechanism should not be labeled with a quantum efficiency. But what about cases where thermal effects enhance the efficiency of a quantum "hot" electron-driven process? To what relative degree can a classical thermal enhancement be before the demarking line is drawn? This conundrum, reminiscent of the ship of Theseus and the Sorites paradoxes, perhaps has no objective answer and motivates the use of noncategorical language, such as OLE, when describing photoefficiency in plasmonic catalysis.

Conclusion

Thermal and nonthermal effects were investigated for CO₂ hydrogenation on plasmonic Rh nanoparticles supported on TiO₂ and Al₂O₃, and for NH₃ synthesis on Ru-Cs/MgO. Nonthermal effects contributed significantly to CO₂ hydrogenation on Rh. On the contrary, in the case of NH₃ synthesis, the rate enhancement from light was due to classical thermal effects, specifically the formation of a favorable thermal gradient. Even when nonthermal effects were confirmed to be significant, photothermal heating still accelerated the nonthermal reaction until the surface temperature was sufficiently high that the detriment to plasmon strength outweighed the kinetic enhancement. Following the establishment of the nonthermal mechanism, three methods were developed to isolate thermal effects from nonthermal effects by our research group. First, the T_e method, where three thermocouples were used to measure temperatures at different locations in the reactor to enable the iterative calculation of a unified descriptor $T_{\rm e}$ to more accurately characterize thermal conditions for the establishment of a more accurate thermal rate; second, the covered/uncovered method, where inert black photothermally active powder was placed atop the catalyst to emulate surface photothermal heating and associated thermal gradients while maintaining dark conditions; and third, the mass dependence test, where the subsurface catalyst was gradually replaced with inert material, methodically decreasing the thermal rate while leaving the nonthermal rate unchanged. The observed trend was then mathematically extrapolated towards zero mass, where the intercept represents only the nonthermal rate. In all cases, the nonthermal rate remained a function of temperature, leading to the conclusion that, while a quantum electron transfer mechanism drives the reaction, it can still be accelerated or impeded by thermal conditions. Thus, the nonthermal rate is not athermal. To account for this reality, a new index OLE was introduced that categorically avoids mislabeling thermal effects as "quantum". The inclusive nature of this index made it suitable for the optimization of both thermal and nonthermal effects, taking into account their constructive and destructive interactions to achieve the maximum photoefficiency for the system studied. Finally, in the case of a purely or mostly nonthermal enhancement mechanism, adjusting production metrics by working area, akin to electrochemistry, where production is commonly adjusted by electrode surface area, may be more appropriate than adjusting by mass, a practice originating in the field of thermal catalysis, where, unlike in plasmonic catalysis, conditions are essentially homogenous.

AUTHOR INFORMATION

Corresponding Author

Jie Liu - Department of Chemistry, Duke University, Durham, NC 27705, United States;

Email: j.liu@duke.edu

Authors

Joey Offen - Department of Chemistry, Duke University, Durham, NC 27705, United States;

Zhijia Geng - Department of Chemistry, Duke University, Durham, NC 27705, United States;

Yifan Yu - Department of Chemistry, Duke University, Durham, NC 27705, United States;

Notes

The authors declare no competing financial interest.

ACKNOWLEDGMENTS

This work was supported by a grant from the National Science Foundation (grant number CHE-1954838). JO was partially supported by a Duke University Nanoscience Fellowship and Energy Fellowship. ZG and YY were also supported, in part, by the Duke University Nanoscience Fellowship.

References

- (1) Christopher, P.; Xin, H.; Linic, S. Visible-Light-Enhanced Catalytic Oxidation Reactions on Plasmonic Silver Nanostructures. *Nature Chemistry* **2011**, *3* (6), 467-472. DOI: 10.1038/nchem.1032.
- (2) Aslam, U.; Rao, V. G.; Chavez, S.; Linic, S. Catalytic Conversion of Solar to Chemical Energy on Plasmonic Metal Nanostructures. *Nature Catalysis* **2018**, *I* (9), 656-665. DOI: 10.1038/s41929-018-0138-x.
- (3) Besteiro, L. V.; Kong, X.-T.; Wang, Z.; Hartland, G.; Govorov, A. O. Understanding Hot-Electron Generation and Plasmon Relaxation in Metal Nanocrystals: Quantum and Classical Mechanisms. *ACS Photonics* **2017**, *4* (11), 2759-2781. DOI: 10.1021/acsphotonics.7b00751.
- (4) Brongersma, M. L.; Halas, N. J.; Nordlander, P. Plasmon-Induced Hot Carrier Science and Technology. *Nature Nanotechnology* **2015**, *10* (1), 25-34. DOI: 10.1038/nnano.2014.311.
- (5) Brown, A. M.; Sundararaman, R.; Narang, P.; Goddard, W. A., III; Atwater, H. A. Nonradiative Plasmon Decay and Hot Carrier Dynamics: Effects of Phonons, Surfaces, and Geometry. *ACS Nano* **2016**, *10* (1), 957-966. DOI: 10.1021/acsnano.5b06199.

- (6) Sundararaman, R.; Narang, P.; Jermyn, A. S.; Goddard Iii, W. A.; Atwater, H. A. Theoretical Predictions for Hot-Carrier Generation from Surface Plasmon Decay. *Nature Communications* **2014**, *5* (1), 5788. DOI: 10.1038/ncomms6788.
- (7) Zhan, C.; Liu, B.-W.; Huang, Y.-F.; Hu, S.; Ren, B.; Moskovits, M.; Tian, Z.-Q. Disentangling Charge Carrier from Photothermal Effects in Plasmonic Metal Nanostructures. *Nature Communications* **2019**, *10* (1), 2671. DOI: 10.1038/s41467-019-10771-3.
- (8) Zhang, X.; Li, X.; Reish, M. E.; Zhang, D.; Su, N. Q.; Gutiérrez, Y.; Moreno, F.; Yang, W.; Everitt, H. O.; Liu, J. Plasmon-Enhanced Catalysis: Distinguishing Thermal and Nonthermal Effects. *Nano Letters* **2018**, *18* (3), 1714-1723. DOI: 10.1021/acs.nanolett.7b04776.
- (9) Kamarudheen, R.; Aalbers, G. J. W.; Hamans, R. F.; Kamp, L. P. J.; Baldi, A. Distinguishing among All Possible Activation Mechanisms of a Plasmon-Driven Chemical Reaction. *ACS Energy Letters* **2020**, *5* (8), 2605-2613. DOI: 10.1021/acsenergylett.0c00989.
- (10) Dubi, Y.; Un, I. W.; Baraban, J. H.; Sivan, Y. Distinguishing Thermal from Non-Thermal Contributions to Plasmonic Hydrodefluorination. *Nature Catalysis* **2022**, *5* (4), 244-246. DOI: 10.1038/s41929-022-00767-6.
- (11) Robatjazi, H.; Bao, J. L.; Zhang, M.; Zhou, L.; Christopher, P.; Carter, E. A.; Nordlander, P.; Halas, N. J. Plasmon-Driven Carbon-Fluorine (C(Sp3)-F) Bond Activation with Mechanistic Insights into Hot-Carrier-Mediated Pathways. *Nature Catalysis* **2020**, *3* (7), 564-573. DOI: 10.1038/s41929-020-0466-5.
- (12) Mascaretti, L.; Naldoni, A. Hot Electron and Thermal Effects in Plasmonic Photocatalysis. *Journal of Applied Physics* **2020**, *128* (4), 041101. DOI: 10.1063/5.0013945.
- (13) Zhou, L.; Swearer, D. F.; Zhang, C.; Robatjazi, H.; Zhao, H.; Henderson, L.; Dong, L.; Christopher, P.; Carter, E. A.; Nordlander, P.; Halas, N. J. Quantifying Hot Carrier and Thermal Contributions in Plasmonic Photocatalysis. *Science* **2018**, *362* (6410), 69-72. DOI: doi:10.1126/science.aat6967.
- (14) Sivan, Y.; Baraban, J.; Un, I. W.; Dubi, Y. Comment on "Quantifying Hot Carrier and Thermal Contributions in Plasmonic Photocatalysis". *Science* **2019**, *364* (6439). DOI: doi:10.1126/science.aaw9367.
- (15) Robatjazi, H.; Schirato, A.; Alabastri, A.; Christopher, P.; Carter, E. A.; Nordlander, P.; Halas, N. J. Reply To: Distinguishing Thermal from Non-Thermal Contributions to Plasmonic Hydrodefluorination. *Nature Catalysis* **2022**, *5* (4), 247-250. DOI: 10.1038/s41929-022-00768-5.
- (16) Jain, P. K. Taking the Heat Off of Plasmonic Chemistry. *The Journal of Physical Chemistry C* **2019**, 123 (40), 24347-24351. DOI: 10.1021/acs.jpcc.9b08143.
- (17) Zhang, X.; Li, X.; Zhang, D.; Su, N. Q.; Yang, W.; Everitt, H. O.; Liu, J. Product Selectivity in Plasmonic Photocatalysis for Carbon Dioxide Hydrogenation. *Nature Communications* **2017**, *8* (1), 14542. DOI: 10.1038/ncomms14542.
- (18) Collado, L.; Reynal, A.; Fresno, F.; Barawi, M.; Escudero, C.; Perez-Dieste, V.; Coronado, J. M.; Serrano, D. P.; Durrant, J. R.; de la Peña O'Shea, V. A. Unravelling the Effect of Charge Dynamics at the Plasmonic Metal/Semiconductor Interface for CO₂ Photoreduction. *Nature Communications* **2018**, *9* (1), 4986. DOI: 10.1038/s41467-018-07397-2.

- (19) Linic, S.; Aslam, U.; Boerigter, C.; Morabito, M. Photochemical Transformations on Plasmonic Metal Nanoparticles. *Nature Materials* **2015**, *14* (6), 567-576. DOI: 10.1038/nmat4281.
- (20) Mubeen, S.; Lee, J.; Singh, N.; Krämer, S.; Stucky, G. D.; Moskovits, M. An Autonomous Photosynthetic Device in Which All Charge Carriers Derive from Surface Plasmons. *Nature Nanotechnology* **2013**, *8* (4), 247-251. DOI: 10.1038/nnano.2013.18.
- (21) Yuan, Y.; Zhou, L.; Robatjazi, H.; Bao, J. L.; Zhou, J.; Bayles, A.; Yuan, L.; Lou, M.; Lou, M.; Khatiwada, S.; Carter, E. A.; Nordlander, P.; Halas, N. J. Earth-Abundant Photocatalyst for H₂ Generation from NH₃ with Light-Emitting Diode Illumination. *Science* **2022**, *378* (6622), 889-893. DOI: doi:10.1126/science.abn5636.
- (22) Fleischmann, M.; Hendra, P. J.; McQuillan, A. J. Raman Spectra of Pyridine Adsorbed at a Silver Electrode. *Chemical Physics Letters* **1974**, *26* (2), 163-166. DOI: https://doi.org/10.1016/0009-2614(74)85388-1.
- (23) Vo-Dinh, T. Surface-Enhanced Raman Spectroscopy Using Metallic Nanostructures. *TrAC Trends in Analytical Chemistry* **1998**, *17* (8), 557-582. DOI: https://doi.org/10.1016/S0165-9936(98)00069-7.
- (24) Kasili, P. M.; Vo-Dinh, T. Photothermal Treatment of Human Carcinoma Cells Using Liposome-Encapsulated Gold Nanoshells. *NanoBiotechnology* **2005**, *I* (3), 245-252. DOI: 10.1385/NBT:1:3:245.
- (25) West, J. L.; Halas, N. J. Engineered Nanomaterials for Biophotonics Applications: Improving Sensing, Imaging, and Therapeutics. *Annual Review of Biomedical Engineering* **2003**, *5* (1), 285-292. DOI: 10.1146/annurev.bioeng.5.011303.120723.
- (26) Linic, S.; Christopher, P.; Ingram, D. B. Plasmonic-Metal Nanostructures for Efficient Conversion of Solar to Chemical Energy. *Nature Materials* **2011**, *10* (12), 911-921. DOI: 10.1038/nmat3151.
- (27) Christopher, P.; Xin, H.; Marimuthu, A.; Linic, S. Singular Characteristics and Unique Chemical Bond Activation Mechanisms of Photocatalytic Reactions on Plasmonic Nanostructures. *Nature Materials* **2012**, *11* (12), 1044-1050. DOI: 10.1038/nmat3454.
- (28) Awazu, K.; Fujimaki, M.; Rockstuhl, C.; Tominaga, J.; Murakami, H.; Ohki, Y.; Yoshida, N.; Watanabe, T. A Plasmonic Photocatalyst Consisting of Silver Nanoparticles Embedded in Titanium Dioxide. *Journal of the American Chemical Society* **2008**, *130* (5), 1676-1680. DOI: 10.1021/ja076503n.
- (29) Chen, X.; Zhu, H.-Y.; Zhao, J.-C.; Zheng, Z.-F.; Gao, X.-P. Visible-Light-Driven Oxidation of Organic Contaminants in Air with Gold Nanoparticle Catalysts on Oxide Supports. *Angewandte Chemie International Edition* **2008**, *47* (29), 5353-5356. DOI: https://doi.org/10.1002/anie.200800602.
- (30) Wang, P.; Huang, B.; Qin, X.; Zhang, X.; Dai, Y.; Wei, J.; Whangbo, M.-H. Ag@Agcl: A Highly Efficient and Stable Photocatalyst Active under Visible Light. *Angewandte Chemie International Edition* **2008**, *47* (41), 7931-7933. DOI: https://doi.org/10.1002/anie.200802483.
- (31) *Plasmonic Catalysis*; Camargo, Pedro H. C.; Cortés, Emiliano; Wiley-VCH: Weinheim, 2021. DOI: 10.1002/9783527826971.
- (32) Frischkorn, C.; Wolf, M. Femtochemistry at Metal Surfaces: Nonadiabatic Reaction Dynamics. *Chemical Reviews* **2006**, *106* (10), 4207-4233. DOI: 10.1021/cr050161r.

- (33) Buntin, S. A.; Richter, L. J.; Cavanagh, R. R.; King, D. S. Optically Driven Surface Reactions: Evidence for the Role of Hot Electrons. *Physical Review Letters* **1988**, *61* (11), 1321-1324. DOI: 10.1103/PhysRevLett.61.1321.
- (34) Cortés, E.; Grzeschik, R.; Maier, S. A.; Schlücker, S. Experimental Characterization Techniques for Plasmon-Assisted Chemistry. *Nature Reviews Chemistry* **2022**, *6* (4), 259-274. DOI: 10.1038/s41570-022-00368-8.
- (35) Baffou, G.; Bordacchini, I.; Baldi, A.; Quidant, R. Simple Experimental Procedures to Distinguish Photothermal from Hot-Carrier Processes in Plasmonics. *Light: Science & Applications* **2020**, *9* (1), 108. DOI: 10.1038/s41377-020-00345-0.
- (36) Sivan, Y.; Baraban, J. H.; Dubi, Y. Experimental Practices Required to Isolate Thermal Effects in Plasmonic Photo-Catalysis: Lessons from Recent Experiments. *OSA Continuum* **2020**, *3* (3), 483-497. DOI: 10.1364/OSAC.376809.
- (37) Li, X.; Everitt, H. O.; Liu, J. Confirming Nonthermal Plasmonic Effects Enhance CO2 Methanation on Rh/TiO₂ Catalysts. *Nano Research* **2019**, *12* (8), 1906-1911. DOI: 10.1007/s12274-019-2457-x.
- (38) Li, X.; Zhang, X.; Everitt, H. O.; Liu, J. Light-Induced Thermal Gradients in Ruthenium Catalysts Significantly Enhance Ammonia Production. *Nano Letters* **2019**, *19* (3), 1706-1711. DOI: 10.1021/acs.nanolett.8b04706.
- (39) Luo, S.; Ren, X.; Lin, H.; Song, H.; Ye, J. Plasmonic Photothermal Catalysis for Solar-to-Fuel Conversion: Current Status and Prospects. *Chemical Science* **2021**, *12* (16), 5701-5719, 10.1039/D1SC00064K. DOI: 10.1039/D1SC00064K.
- (40) Marimuthu, A.; Zhang, J.; Linic, S. Tuning Selectivity in Propylene Epoxidation by Plasmon Mediated Photo-Switching of Cu Oxidation State. *Science* **2013**, *339* (6127), 1590-1593.
- (41) La Mer, V. K. Chemical Kinetics. The Temperature Dependence of the Energy of Activation. The Entropy and Free Energy of Activation. *The Journal of Chemical Physics* **1933**, *1* (5), 289-296. DOI: 10.1063/1.1749291.
- (42) Avanesian, T.; Gusmão, G. S.; Christopher, P. Mechanism of CO₂ Reduction by H2 on Ru(0001) and General Selectivity Descriptors for Late-Transition Metal Catalysts. *Journal of Catalysis* **2016**, *343*, 86-96. DOI: https://doi.org/10.1016/j.jcat.2016.03.016.
- (43) Zhang, X.; Li, P.; Barreda, Á.; Gutiérrez, Y.; González, F.; Moreno, F.; Everitt, H. O.; Liu, J. Size-Tunable Rhodium Nanostructures for Wavelength-Tunable Ultraviolet Plasmonics. *Nanoscale Horizons* **2016**, *I* (1), 75-80, 10.1039/C5NH00062A. DOI: 10.1039/C5NH00062A.
- (44) Dupré, O.; Vaillon, R.; Green, M. A. Thermal Behavior of Photovoltaic Devices. *Physics and Engineering* **2017**, *10*, 978-973.
- (45) Vaillon, R.; Dupré, O.; Cal, R. B.; Calaf, M. Pathways for Mitigating Thermal Losses in Solar Photovoltaics. *Scientific Reports* **2018**, *8* (1), 13163. DOI: 10.1038/s41598-018-31257-0.
- (46) Geng, Z.; Yu, Y.; Offen, A. J.; Liu, J. Achieving Maximum Overall Light Enhancement in Plasmonic Catalysis by Combining Thermal and Non-Thermal Effects. *Nature Catalysis* **2023**. DOI: 10.1038/s41929-023-01045-9.

- (47) Hegedus, S. Review of Photovoltaic Module Energy Yield (Kwh/Kw): Comparison of Crystalline Si and Thin Film Technologies. *WIREs Energy and Environment* **2013**, *2* (2), 218-233. DOI: https://doi.org/10.1002/wene.61.
- (48) Swearer, D. F.; Zhao, H.; Zhou, L.; Zhang, C.; Robatjazi, H.; Martirez, J. M. P.; Krauter, C. M.; Yazdi, S.; McClain, M. J.; Ringe, E.; Carter, E. A.; Nordlander, P.; Halas, N. J. Heterometallic Antenna–Reactor Complexes for Photocatalysis. *Proceedings of the National Academy of Sciences* **2016**, *113* (32), 8916-8920. DOI: 10.1073/pnas.1609769113.
- (49) Elias, R. C.; Linic, S. Elucidating the Roles of Local and Nonlocal Rate Enhancement Mechanisms in Plasmonic Catalysis. *Journal of the American Chemical Society* **2022**, *144* (43), 19990-19998. DOI: 10.1021/jacs.2c08561.
- (50) Kim, Y.; Smith, J. G.; Jain, P. K. Harvesting Multiple Electron–Hole Pairs Generated through Plasmonic Excitation of Au Nanoparticles. *Nature Chemistry* **2018**, *10* (7), 763-769. DOI: 10.1038/s41557-018-0054-3.
- (51) Singh, S.; Verma, R.; Kaul, N.; Sa, J.; Punjal, A.; Prabhu, S.; Polshettiwar, V. Surface Plasmon-Enhanced Photo-Driven CO₂ Hydrogenation by Hydroxy-Terminated Nickel Nitride Nanosheets. *Nature Communications* **2023**, *14* (1), 2551. DOI: 10.1038/s41467-023-38235-9.
- (52) Dubi, Y.; Un, I. W.; Sivan, Y. Thermal Effects an Alternative Mechanism for Plasmon-Assisted Photocatalysis. *Chemical Science* **2020**, *11* (19), 5017-5027, 10.1039/C9SC06480J. DOI: 10.1039/C9SC06480J.
- (53) Ross, J. R. H. Chapter 8 Mass and Heat Transfer Limitations and Other Aspects of the Use of Large-Scale Catalytic Reactors. In *Contemporary Catalysis*, Ross, J. R. H. Ed.; Elsevier, 2019; pp 187-213.
- (54) Duhr, S.; Braun, D. Why Molecules Move Along a Temperature Gradient. *Proceedings of the National Academy of Sciences of the United States of America* **2006**, *103* (52), 19678-19682.